Supplementary Information

A seeding strategy enables catalyst-free high-rate lithium–oxygen batteries

Rongze Sun,[‡a] Wenjie Niu,[‡a] Ning Zhao,*[a] Pengfei Yu,*[b] and Xiangxin Guo*[a]

a. College of Physics, Qingdao University, Qingdao 266071, China.
E-mail: n.zhao@qdu.edu.cn; xxguo@qdu.edu.cn

b. Center for Transformative Science, ShanghaiTech University, Shanghai 201210, China.
E-mail: yupf1@shanghaitech.edu.cn

‡ These authors contributed equally to this work.

Experimental Section

The Vertically aligned carbon nanotube (VACNT) cathodes grown on stainless steel mesh were purchased from Microphase Co. LTD, Japan. The mass loading of the VACNTs was approximately 2.0 mg cm^{-2}, and the specific surface area was approximately 80 m^2 g^{-1}.

Swagelok-type batteries were assembled in an argon-filled glovebox with oxygen and moisture levels maintained below 0.1 ppm. The battery components consisted of a lithium foil anode, a VACNT cathode, and a glass fiber separator (purchased from Whatman) impregnated with the electrolyte.

The morphological evolution of the cathodes after discharge at various oxygen pressures and current densities was examined using a scanning electron microscope (SEM, Hitachi S-4800, Japan). To investigate the microstructure of the seeding sites formed at the initial stage of discharge, spherical aberration-corrected high-resolution transmission electron microscopy (HR-TEM, JEOL JEM-2100F) was utilized. X-ray diffraction (XRD) analysis of the discharge products was performed using a Bruker D8 Discover diffractometer equipped with a Cu Kα radiation source.

Galvanostatic charge-discharge tests were conducted using a NEWARE battery testing system (CT-4008Tn). The Swagelok-type batteries were placed in a gas-controllable airtight chamber and tested at various current densities under different oxygen pressures. Electrochemical impedance spectroscopy (EIS) measurements were performed on a PARSTAT 3000A electrochemical workstation (Princeton Applied Research) within a frequency range from 100 kHz to 0.1 Hz.

Computational details

All of the calculations are performed in the framework of the density functional theory with the projector augmented plane-wave method, as implemented in the Vienna ab initio simulation package (VASP)[1,2]. The generalized gradient approximation (GGA) proposed by Perdew, Burke, and Ernzerhof (PBE) is selected for the exchange-correlation potential[3,4]. The long-range van der Waals interaction is described by the

DFT-D3 approach[5]. The cut-off energy for plane wave is set to 520 eV. The energy criterion is set to 10^{-4} eV in iterative solution of the Kohn-Sham equation. The Brillouin zone integrations for Li_2O_2 (0 0 1), Li_2O_2 (1 1 0), Li_2O_2 (1 0 1), Li_2O_2 (1 0 0), CNT, CNT-O_2 and CNT-Li_2O_2 are performed using 3×3×1, 3×2×1, 3×3×1 ,3×3×1, 3×3×1, 3×3×1 and 3×3×1 k-meshes, respectively. All the structures are relaxed until the residual forces on the atoms have declined to less than 0.05 eV/Å. Data analysis and visualization are carried out with the help of VASPKIT[6] code and VESTA[7]. To avoid interlaminar interactions, a vacuum spacing of 20 Å is applied perpendicular to the slab.

The surface energy can be defined by the equation:

$$E_{surface} = \frac{(E_{slab} - NE_{bulk})}{2A}$$

In the equation, E_{slab} is the total energy of the relaxed slab materials, $E_{bulk}$is the energy per unit formula of the bulk, N stands for E_{slab} multiple of E_{bulk}, A_{slab} is the total area of slab materials.

Here, differences in Gibbs free energy (ΔG) for intermediates defined as:

$$\Delta G = \Delta E + \Delta E_{ZPE} - T\Delta S$$

where ΔE is the total energy difference between the slab and respective terminations computed by DFT-PBE. ΔE_{ZPE} and $T\Delta S$ denotes differences in zero-point energy and entropy between adsorbed states of reaction intermediates and gap phase, respectively. T is the room temperature (298.15 K).

The adsorption energy Eads is expressed as :

$$\Delta E_{\text{ads}} = E_{\text{A+B}} - E_{\text{A}} - E_{\text{B}}$$

where E_{A+B} is the total energy of slab A model with B adsorption, E_A is the energy of a A slab, and E_B is that for a B molecule.

Supporting Figures

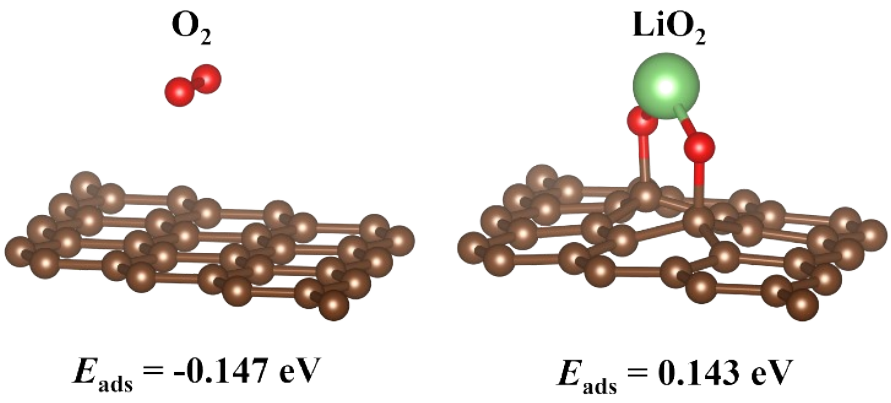

Fig. S1 DFT optimized structure models and adsorption energies of O_2 and LiO_2 on VACNT surface under 1atm O_2.

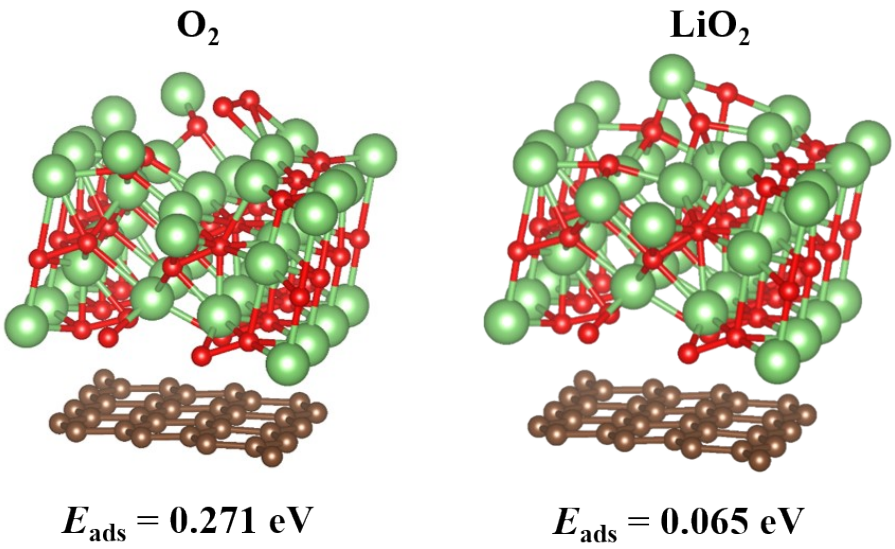

Fig. S2 DFT optimized structure models and adsorption energies of O_2 and LiO_2 on VACNT-Li_2O_2 surface under 1atm O_2.

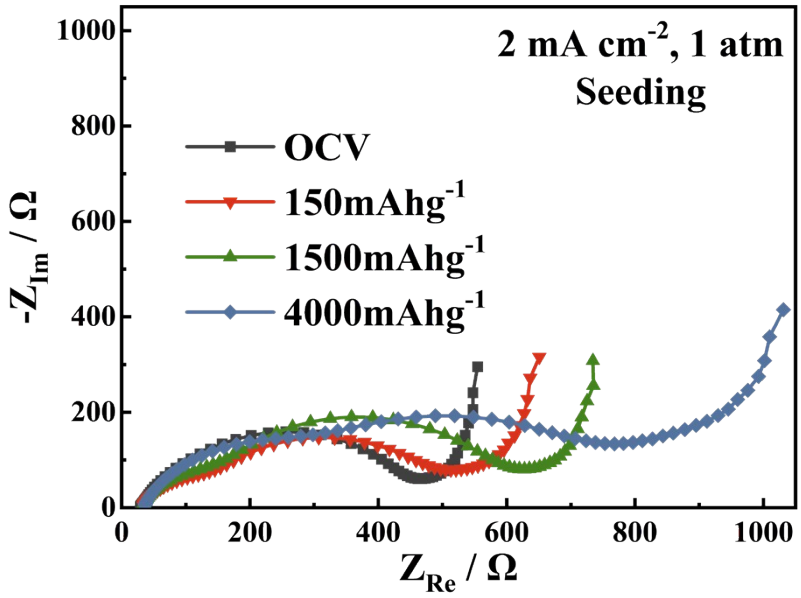

Fig. S3 The electrochemical impedance spectroscopy (EIS) evolution of the seeded cathode during discharge at 2 mA cm^{-2}.

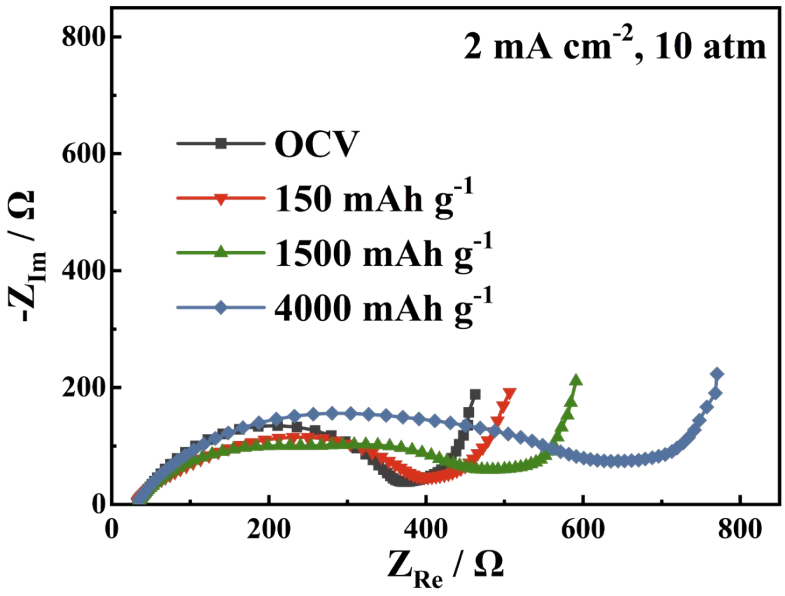

Fig. S4 The EIS evolution at various discharge stages under 10 atm and 2 mA cm^{-2}.

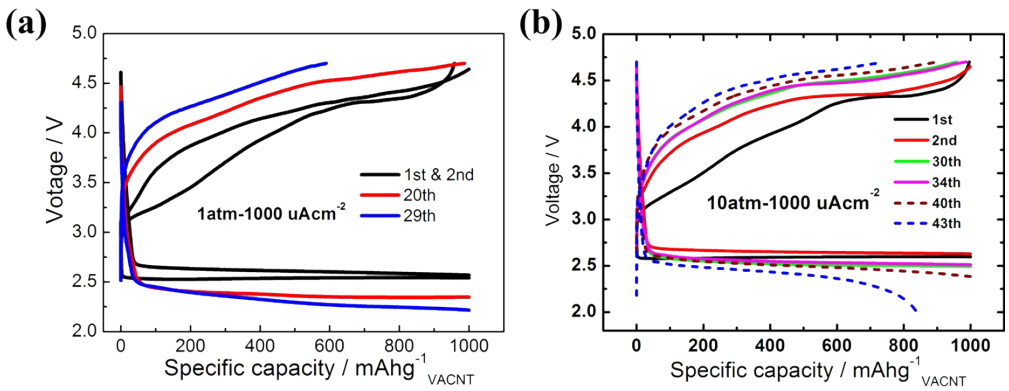

Fig. S5 Cycling performance at 1atm and 10atm under a current density of 1.0 mA cm^{-2} with a controlled discharge/charge depth of 1000 mAh g^{-1}.

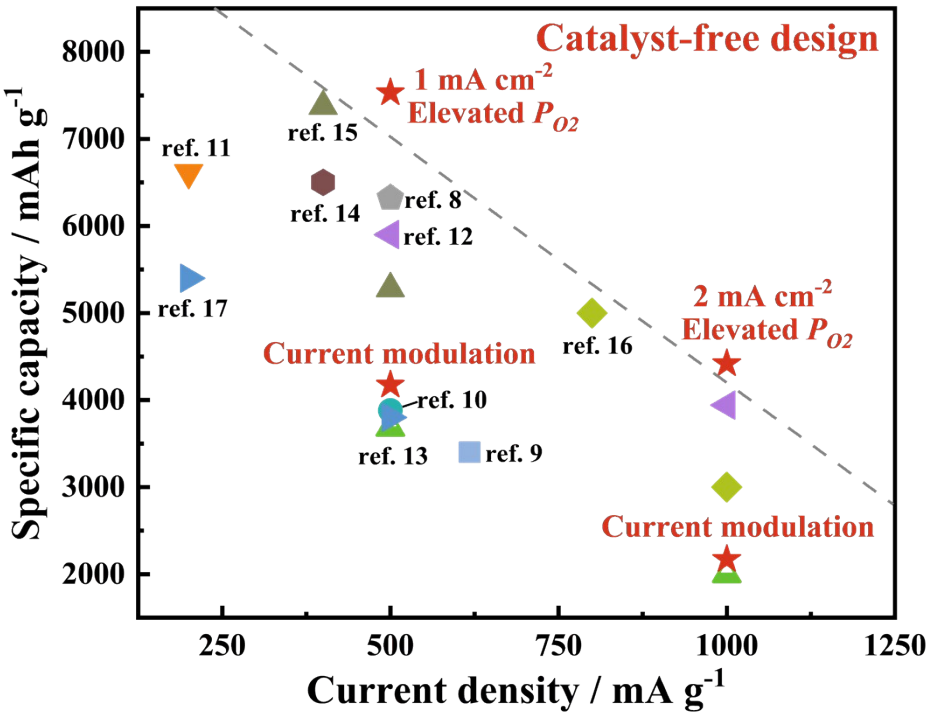

Fig. S6 Comparative analysis of catalyst-based studies[8-17] and the present catalyst-free strategy on specific capacity under high current density.

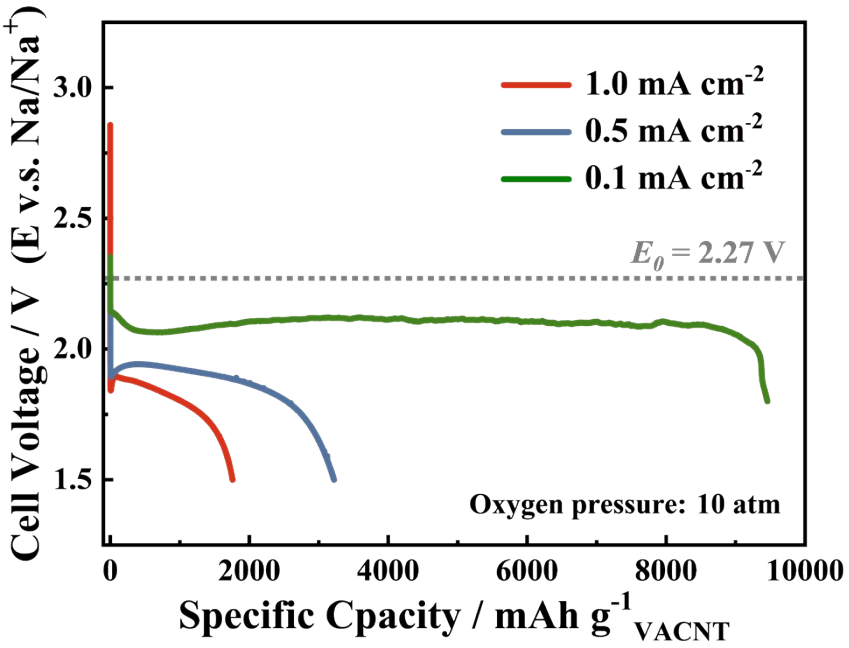

Fig. S7 Discharge performance of the Na-O_2 battery at varying current densities under 10 atm O_2.

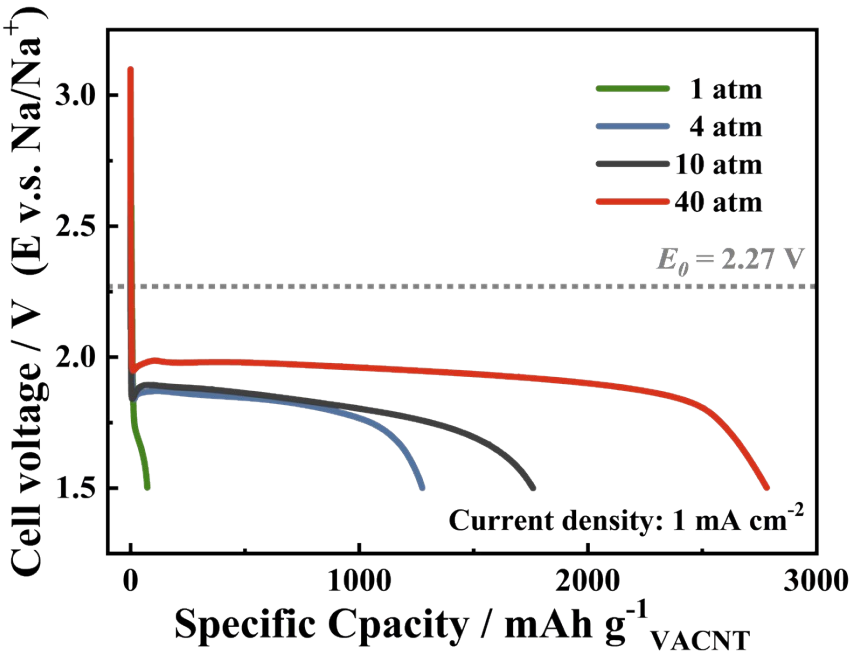

Fig. S8 Oxygen pressure dependence of the discharge capacity for the Na-O_2 battery measured at 1 mA cm^{-2}.

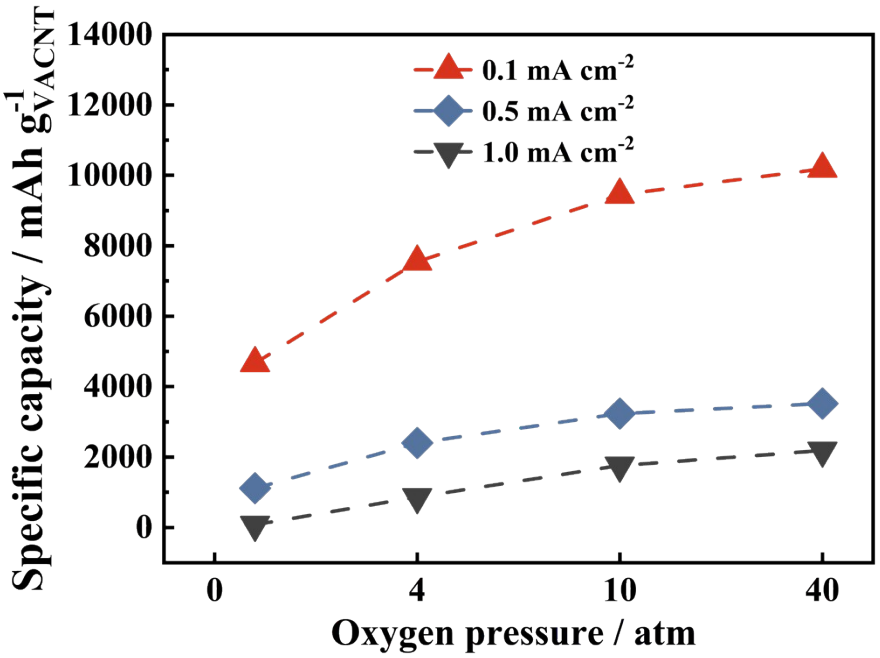

Fig. S9 Evolution of the discharge capacity in the Na-O_2 batteries under varying current densities and oxygen pressures.

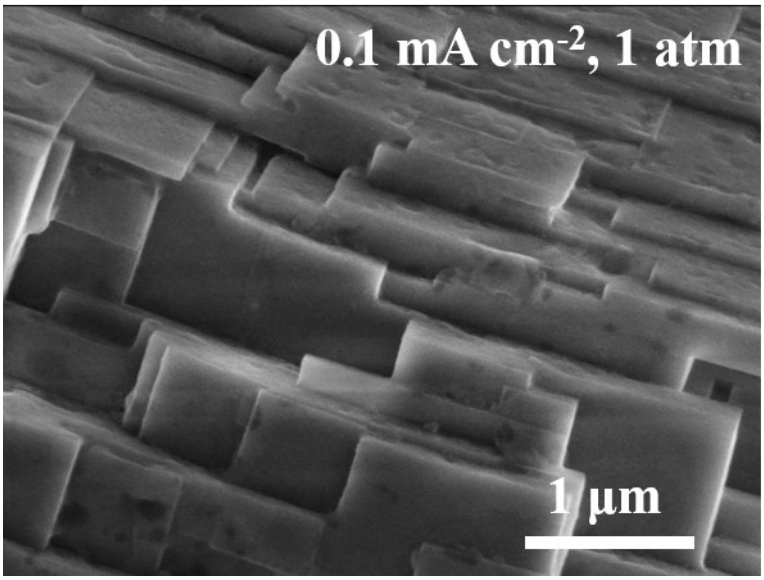

Fig. S10 Morphology of the discharge products in the Na-O_2 battery at 1 atm O_2.

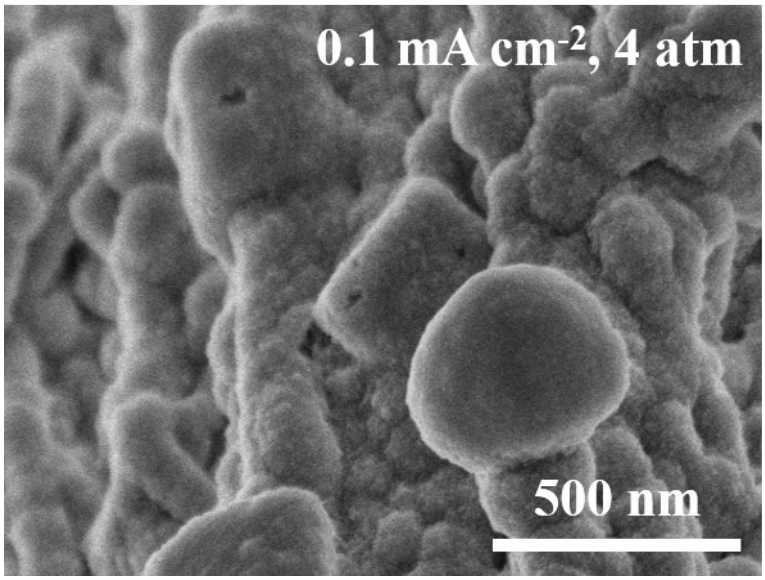

Fig. S11 Morphology of the discharge products in the Na-O_2 battery at 4 atm O_2.

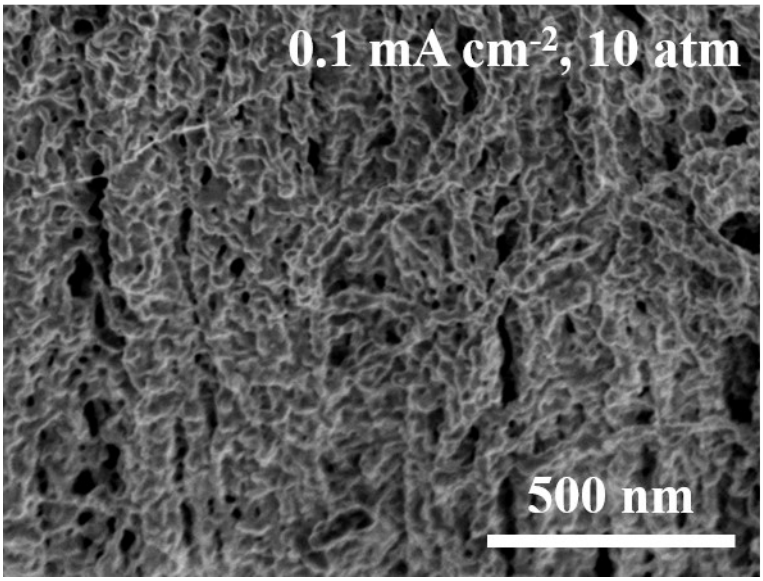

Fig. S12 Morphology of the discharge products in the Na-O_2 battery at 10 atm O_2.

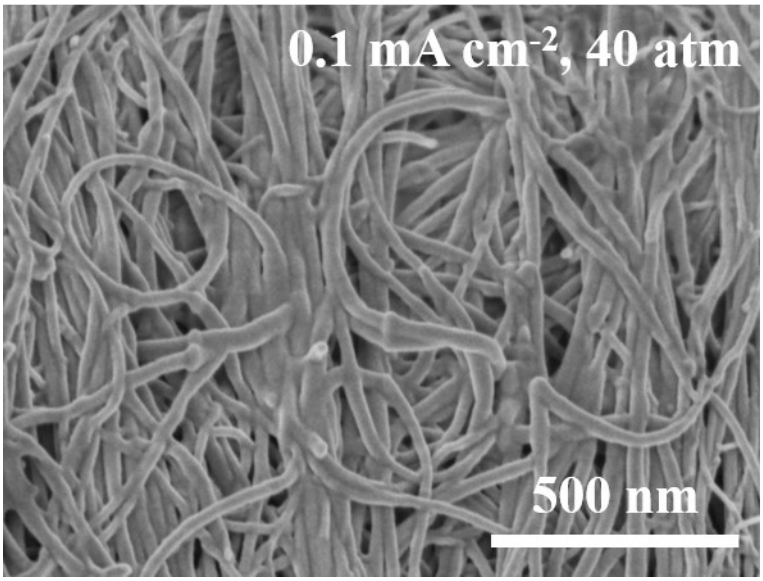

Fig. S13 Morphology of the discharge products in the Na-O_2 battery at 40 atm O_2.

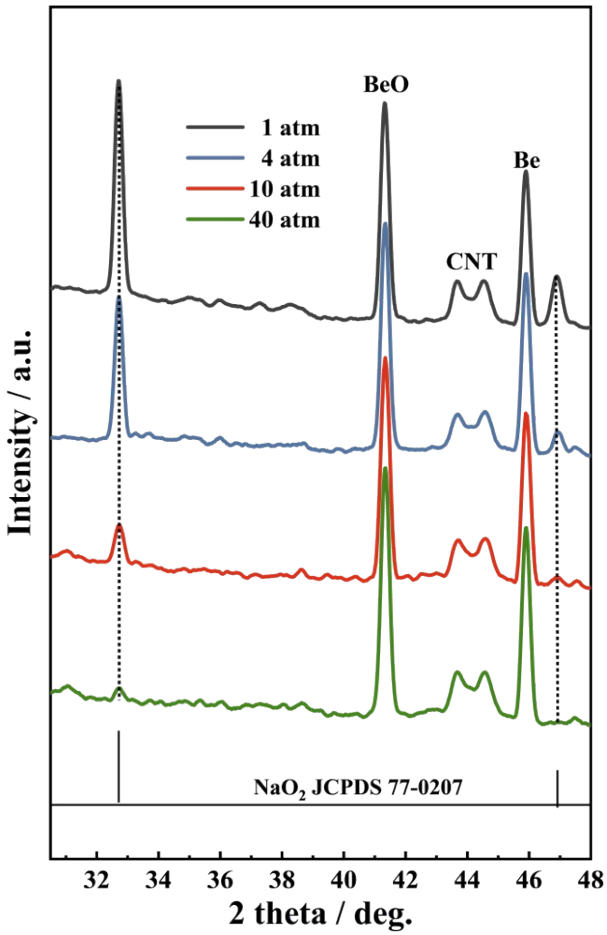

Fig. S14 XRD patterns of the discharge products for the Na-O_2 battery under different oxygen pressures.

References

1 Kresse, G. & Hafner, J. Ab initio molecular dynamics for open-shell transition metals. *Phys. Rev. B Condens. Matter*, 1993, **48**, 13115-13118.

2 Kresse, G. F. l., J. Efficient iterative schemes for ab initio total-energy calculations using a plane-wave basis set. *Phys. Rev. B Condens. Matter*, 1996, **54**, 169-185.

3 John P. Perdew, K. B., and Matthias Ernzerhof. Generalized gradient approximation made simple. *Phys. Rev. Lett*, 1996, **77**.

4 Kohn, W. & Sham, L. J. Self-Consistent Equations Including Exchange and Correlation Effects. *Phys. Rev.*, 1965, **140**, A1133-A1138.

5 Grimme, S., Antony, J., Ehrlich, S. & Krieg, H. A consistent and accurate ab initio parametrization of density functional dispersion correction (DFT-D) for the 94 elements H-Pu. *J. Chem. Phys*, 2010, **132**, 154104.

6 Wang, V., Xu, N., Liu, J.-C., Tang, G. & Geng, W.-T. VASPKIT: A user-friendly interface facilitating high-throughput computing and analysis using VASP code. *Comput. Phys. Commun.,* 2021, **267**, 108033.

7 Momma, K. & Izumi, F. VESTA: a three-dimensional visualization system for electronic and structural analysis. *J. Appl. Crystallogr.*, 2008, **41**, 653-658.

8 Y. Wang, S. Ma, M. Li, H. Liu, B. Huo, K. Zeng and Z. Sun, *J. Cleaner Prod.*, 2026, **554**, 148144.

9 P. Zhang, S. Zhang, M. He, J. Lang, A. Ren, S. Xu and X. Yan, *Adv. Sci.*, 2017, **4**, 1700172.

10 Y. Yao, S. Wang, X. Ma, Y. Han, Z. Tong, G. Li, J. Feng, M. D. Khan, N. Revaprasadu, Q. Sun and Y. Tian, *Small*, 2025, **21**, 2503521.

11 P. Xia, H. Wu, H. Yuan, X. Yang, T. Xia, J. Ma, Y. Yuan and Y. Dong, *J. Energy Storage*, 2025, **133**, 118082.

12 R. Zhang, T. S. Zhao, M. Wu, P. Tan and H. Jiang, *Energy Technol.*, 2018, **6**, 263-272.

13 A. Hu, W. Lv, T. Lei, W. Chen, Y. Hu, C. Shu, X. Wang, L. Xue, J. Huang, X. Du, H. Wang, K. Tang, C. Gong, J. Zhu, W. He, J. Long and J. Xiong, *ACS Nano*, 2020, **14**, 3490-3499.

14 Y. Niu, Y. Feng, C. Su, C. Wu, S. Zhang, Z. Lu, W. Xia, R. Ma, M. Ma, K. Xia, H. Xue and H. Gong, *Chem. Eng. J.*, 2025, **525**, 170542.

15 Z. Zhou, B. Li, J. Li, K. Wang, J. Bi, S. He, X. Yu, W. Ai and W. Huang, *Adv. Mater.*, 2026, **38**, e72632.

16 S. Guan, W. Jia, Y. Gao, M. Liu, L. Wang, Y. Zhu and X. Li, *Angew. Chem., Int. Ed.*, 2026, **65**, e23729.

17 Y. Yao, S. Wang, X. Ma, Y. Han, Z. Tong, G. Li, J. Feng, M. D. Khan, N. Revaprasadu, Q. Sun and Y. Tian, *Small*, 2025, **21**, 2503521.